Research Article | Vol. 7, No. 12 | 1 Dec 2016 | BIOMEDICAL OPTICS EXPRESS 5308

Biomedical Optics EXPRESS

Imaging behind opaque obstacle: a potential method for guided *in vitro* needle placement

SANDEEP MENON PERINCHERY, ANANT SHINDE, AND MURUKESHAN VADAKKE MATHAM*

School of Mechanical and Aerospace Engineering, Nanyang Technological University, Centre for Optical and Laser Engineering, 50 Nanyang Avenue, 639798, Singapore
*mmurukeshan@ntu.edu.sg

Abstract: We report a simple real time optical imaging concept using an axicon lens to image the object kept behind opaque obstacles in free space. The proposed concept underlines the importance and advantages of using an axicon lens compared to a conventional lens to image behind the obstacle. The potential of this imaging concept is demonstrated by imaging the insertion of surgical needle in biological specimen in real time, without blocking the field of view. It is envisaged that this proposed concepts and methodology can make a telling impact in a wide variety of areas especially for diagnostics, therapeutics and microscopy applications.

© 2016 Optical Society of America

OCIS codes: (110.0110) Imaging systems; (170.0170) Medical optics and biotechnology.

References and links

1. "WHO Guidelines Approved by the Guidelines Review Committee," in WHO Guideline on the Use of Safety-Engineered Syringes for Intramuscular, Intradermal and Subcutaneous Injections in Health-Care Settings, (World Health Organization 2015. Geneva, 2015).
2. K. J. Connolly, *Psychobiology of the Hand* (Cambridge University Press, 1998).
3. J. H. McLeod, "The Axicon: A New Type of Optical Element," J. Opt. Soc. Am. **44**, 592 (1954).
4. J. W. Y. Lit and R. Tremblay, "Focal depth of a transmitting axicon," J. Opt. Soc. Am. **63**, 445–449 (1973).
5. W. T. Welford, "Use of Annular Apertures to Increase Focal Depth," J. Opt. Soc. Am. **50**, 749–752 (1960).
6. O. Katz, E. Small, and Y. Silberberg, "Looking around corners and through thin turbid layers in real time with scattered incoherent light," Nat. Photonics **6**, 549–553 (2012).
7. I. Thanopulos, D. Luckhaus, T. C. Preston, and R. Signorell, "Dynamics of submicron aerosol droplets in a robust optical trap formed by multiple Bessel beams," J. Appl. Phys. **115**, 154304 (2014).
8. A. Dudley, T. Mhlanga, M. Lavery, A. McDonald, F. S. Roux, M. Padgett, and A. Forbes, "Efficient sorting of Bessel beams," Opt. Express **21**(1), 165–171 (2013).
9. F. O. Fahrbach, P. Simon, and A. Rohrbach, "Microscopy with self-reconstructing beams," Nat. Photonics **4**, 780–785 (2010).
10. K. M. Khan, S. K. Majumder, and P. K. Gupta, "Cone-shell Raman spectroscopy (CSRS) for depth-sensitive measurements in layered tissue," J. Biophotonics **8**(11-12), 889–896 (2015).
11. C. Snoeyink and S. Wereley, "Single-image far-field subdiffraction limit imaging with axicon," Opt. Lett. **38**(5), 625–627 (2013).
12. S. M. Perinchery, A. Shinde, C. Y. Fu, X. J. Jeesmond Hong, M. Baskaran, T. Aung, and V. M. Murukeshan, "High resolution iridocorneal angle imaging system by axicon lens assisted gonioscopy," Sci. Rep. **6**, 30844 (2016).
13. V. Garcés-Chávez, D. McGloin, H. Melville, W. Sibbett, and K. Dholakia, "Simultaneous micromanipulation in multiple planes using a self-reconstructing light beam," Nature **419**(6903), 145–147 (2002).
14. K. Chikuma, S. Okamoto, T. Tohma, and S. Umegaki, "Collimating properties of an axicon for the Čerenkov-radiation-type second-harmonic light from a crystal-cored fiber," Appl. Opt. **33**(15), 3198–3202 (1994).
15. J. O. Stoner, Jr., "Properties of Axicon Systems for Collecting Foil-Excited Accelerator Beam Spectra," Appl. Opt. **9**(1), 53–57 (1970).
16. J. Zheng, Y. Yang, M. Lei, B. Yao, P. Gao, and T. Ye, "Fluorescence volume imaging with an axicon: simulation study based on scalar diffraction method," Appl. Opt. **51**(30), 7236–7245 (2012).
17. G. Druart, J. Taboury, N. Guérineau, R. Haïdar, H. Sauer, A. Kattnig, and J. Primot, "Demonstration of image-zooming capability for diffractive axicons," Opt. Lett. **33**(4), 366–368 (2008).
18. Z. Zhai, S. Ding, Q. Lv, X. Wang, and Y. Zhong, "Extended depth of field through an axicon," J. Mod. Opt. **56**, 1304–1308 (2009).
19. A. Saikaley, B. Chebbi, and I. Golub, "Imaging properties of three refractive axicons," Appl. Opt. **52**(28), 6910–6918 (2013).

#274167 http://dx.doi.org/10.1364/BOE.7.005308
Journal © 2016 Received 22 Aug 2016; revised 21 Nov 2016; accepted 21 Nov 2016; published 29 Nov 2016

Biomedical Optics EXPRESS

20. Z. Bouchal, J. Wagner, and M. Chlup, "Self-reconstruction of a distorted nondiffracting beam," Opt. Commun. **151**, 207–211 (1998).
21. T. A. Planchon, L. Gao, D. E. Milkie, M. W. Davidson, J. A. Galbraith, C. G. Galbraith, and E. Betzig, "Rapid three-dimensional isotropic imaging of living cells using Bessel beam plane illumination," Nat. Methods **8**(5), 417–423 (2011).
22. O. Katz, E. Small, and Y. Silberberg, "Looking through walls and around corners with incoherent light: Wide-field real-time imaging through scattering media," https://arxiv.org/ftp/arxiv/papers/1202/1202.2078.pdf (2012).
23. R. S. Bennink, S. J. Bentley, and R. W. Boyd, "Two-Photon" Coincidence Imaging with a Classical Source," Phys. Rev. Lett. **89**(11), 113601 (2002).
24. M. Rueckel, J. A. Mack-Bucher, and W. Denk, "Adaptive wavefront correction in two-photon microscopy using coherence-gated wavefront sensing," Proc. Natl. Acad. Sci. U.S.A. **103**(46), 17137–17142 (2006).
25. M. J. Booth, D. Débarre, and A. Jesacher, "Adaptive Optics for Biomedical Microscopy," Opt. Photonics News **23**, 22–29 (2012).
26. J. Bertolotti, E. G. van Putten, C. Blum, A. Lagendijk, W. L. Vos, and A. P. Mosk, "Non-invasive imaging through opaque scattering layers," Nature **491**(7423), 232–234 (2012).
27. K. Wu, Q. Cheng, Y. Shi, H. Wang, and G. P. Wang, "Hiding scattering layers for noninvasive imaging of hidden objects," Sci. Rep. **5**, 8375 (2015).
28. R. Arimoto, C. Saloma, T. Tanaka, and S. Kawata, "Imaging properties of axicon in a scanning optical system," Appl. Opt. **31**(31), 6653–6657 (1992).
29. J. S. Choi and J. C. Howell, "Paraxial ray optics cloaking," Opt. Express **22**(24), 29465–29478 (2014).
30. H. Chen, B. Zheng, L. Shen, H. Wang, X. Zhang, N. I. Zheludev, and B. Zhang, "Ray-optics cloaking devices for large objects in incoherent natural light," Nat. Commun. **4**, 2652 (2013).
31. X. Chen, Y. Luo, J. Zhang, K. Jiang, J. B. Pendry, and S. Zhang, "Macroscopic invisibility cloaking of visible light," Nat. Commun. **2**, 176 (2011).
32. X. Ni, Z. J. Wong, M. Mrejen, Y. Wang, and X. Zhang, "An ultrathin invisibility skin cloak for visible light," Science **349**(6254), 1310–1314 (2015).
33. R. Fleury, F. Monticone, and A. Alù, "Invisibility and Cloaking: Origins, Present, and Future Perspectives," Phys. Rev. Appl. **4**, 037001 (2015).
34. U. Leonhardt, "Optical conformal mapping," Science **312**(5781), 1777–1780 (2006).
35. J. B. Pendry, D. Schurig, and D. R. Smith, "Controlling electromagnetic fields," Science **312**(5781), 1780–1782 (2006).

1. Introduction

Despite the advancements in optical technology and optics based imaging schemes, it has been hitherto impossible when the sample or test target needs to be imaged behind opaque objects. For instance, most frequently used medical procedure is injection, with an estimated 20 billion injections administered each year worldwide [1]. There are needle injuries (cuts) reported due to blind injection or improper position of needle caused due to the blocking of the field of view of the sample by the needle during insertion. There are also reports where the surgical tools obstruct the field of view, especially when dealing with extremely small structures [2]. Therefore there is a critical need for designing imaging systems which can image behind opaque obstacles for many such applications.

Axicon lens which was introduced by Macleod [3] in the mid 1950's has been one of the primarily used optical element to illustrate self-reconstruction property of light beams [4, 5]. Self-reconstruction beams have the property to reconstruct by the interfering beams after being partially obstructed by an obstacle. Bessel beam is one such beam type which has the remarkable characteristics of diffraction free propagation with the self-reconstruction ability [6], which made it an excellent candidate in a wide range of applications [7, 8] such as optical imaging, atom tweezing, information extraction, metrology.

Axicon lenses in recent years, specifically in the area of microscopy have been principally utilized to image deeper into inhomogeneous scattering media [9, 10] as well as to attain high resolution imaging [11, 12]. In a notable study, using axicon lens phenomenon of light beam reconstruction after propagating through a plane of beads or a suspension of small beads was demonstrated [13]. In addition to generation of non-diffracting Bessel like beams, axicon lens also enables collimation of conical wave fronts efficiently [14]. In fact, there are studies which have utilized axicon lens specifically as an optical element for improving the collection efficiency of light [15].

Biomedical Optics EXPRESS

A recent article by Stoner *et al.* indicates, through simulations, that an axicon lens can collect the fluorescence from the optical axis and concentrate into a single spot which enables fluorescence volume imaging [16]. Another interesting feature of axicon lens is its extended focal depth and this feature has been used in many studies [17–20]. Though axicon lens has these interesting features, they have not been relatively explored to its potential in the imaging context of viewing behind opaque obstacles. On the contrary, modern microscopy research focuses on improving the spatial, temporal and axial resolutions [21].

In this article, we demonstrate for the first time how to image behind opaque obstacles, blocking the field of view during imaging in free space using a single axicon lens. The imaging concept is demonstrated in three different configurations: transillumination, reflection and fluorescence mode. We have performed optical ray tracing using Zemax and experimental demonstrations to address the advantages of axicon lens over the conventional lens while imaging behind an opaque obstacle in real time. Using an axicon lens, real time imaging behind obstacles having different shapes, sizes and textures are carried out with white light (incoherent) and laser beam (coherent) sources. The proof of concept of using this imaging concept is demonstrated by circumventing the blocking of view by the surgical needle during needle insertion.

2. Materials and methods

2.1 Optical configuration

In this study, we have used three different optical schemes using axicon lens to demonstrate imaging capability behind an obstacle in free space: reflectance, transillumination and fluorescence (Fig. 1). In all these experimental configurations, axicon lens (AX255-A, Apex angle 170°, Material: UVFS, Thorlabs) have been used. In fact, we have used axicon lens with different apex angles such as 110°, 140°, 160° and 170°. However, as we require a large depth of focus (DOF), it is found that the apex angle with 170° is more suitable for this study. For the reflection and fluorescence imaging, the illumination and imaging are performed through the same axicon lens (Fig. 1(a) and Fig. 1(c)). On the contrary, for the transillumination configuration, only imaging is done through the axicon lens and the illumination is provided separately as shown in Fig. 1(b). Both white light (Correct Shimadzu FA-150EN Fiber Illuminator, Japan) and a 488 nm continuous wave laser (Coherent Inc.) are used as illumination sources for trans-illumination and reflection, and fluorescent imaging respectively(Fig. 1(c)). The axicon lens and tube lens were separated by 8 cm (fixed position). A tube lens (ITL200, Thorlabs) is used before the camera for effective light collection. The emitted fluorescence is collected through an emission filter (LPD01-488RS Semrock, Rochester, New York) and imaged by the camera. All the images were captured by Andor iXon3 EMCCD camera. The camera was positioned at the focus position of the tube lens (14.8 cm).

2.2 Materials

For the resolution experiments, the test sample used was a 1951 USAF test chart (2” x 2” USAF Glass Slide Resolution Target, Edmund Optics). We have used the fixed mouse kidney sections (Life Technologies, Inc.) as the test samples. The mouse kidney section was labeled with the fluorescent dye, Alexa Fluor 488 wheat germ agglutinin ($\lambda_{Ex\ Peak}$ = 490 nm, $\lambda_{Em\ Peak}$ = 525 nm).

We have also utilized Zemax software to perform optical ray tracing and ImageJ software for performing image contrast enhancements.

Biomedical Optics EXPRESS

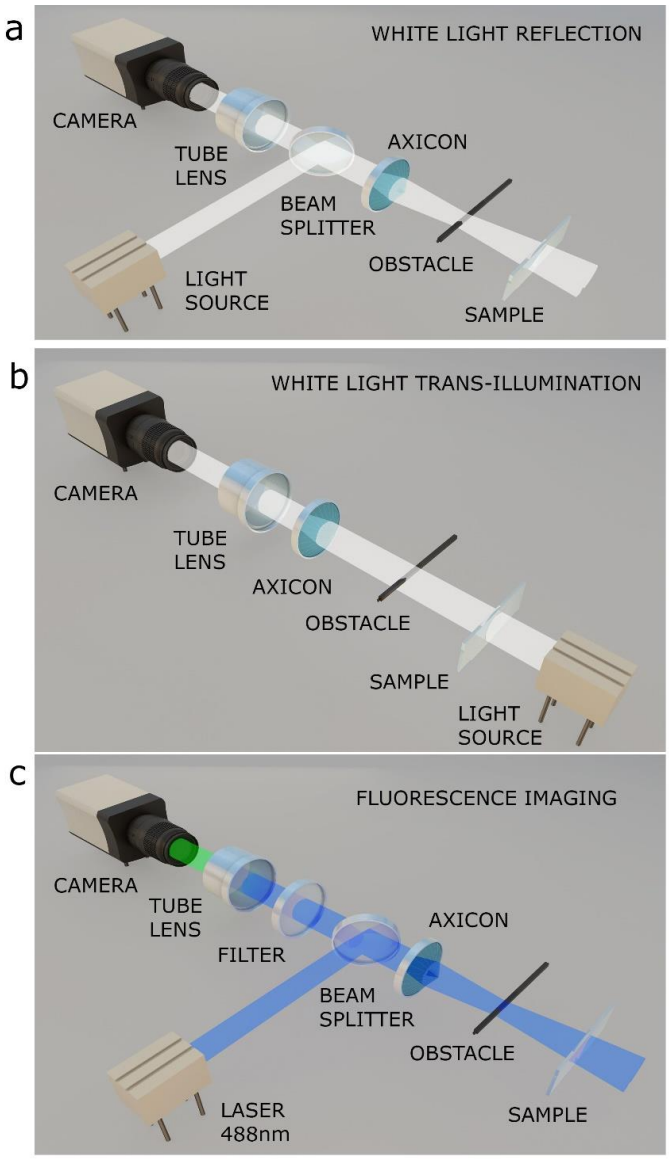

Fig. 1. Optical configuration using axicon lens. (a) Reflection imaging. (b) Trans-illumination. (c) Fluorescence imaging. (Distance between the components are not representative. Exact distances are mentioned in the section 2.1.

Biomedical Optics EXPRESS

3. Results

3.1 Comparison of axicon lens with conventional lens

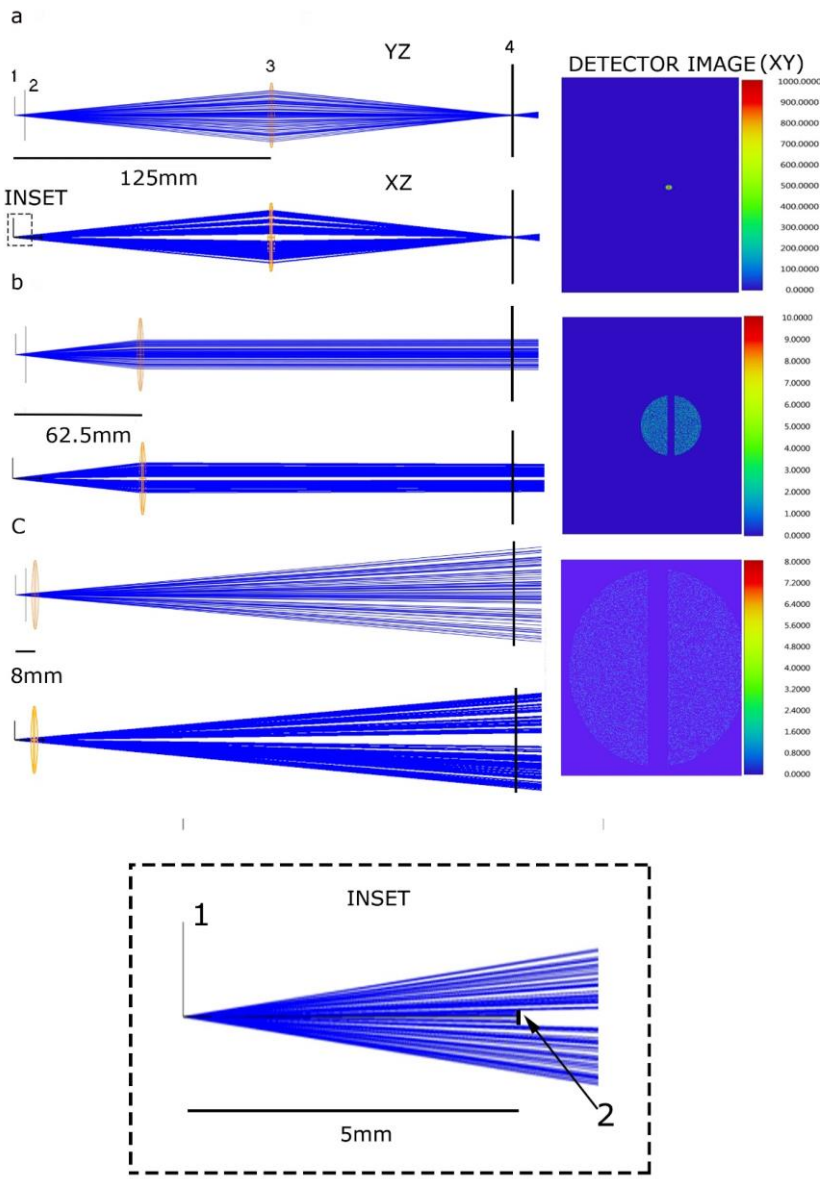

Fig. 2. Illustration of image formation (point source) behind an obstacle for the conventional lens at different focus depth. (a) Ray diagram and detector view for the biconvex lens (LB1904 - N-BK7 Bi-Convex Lens, f = 125 mm, Thorlabs) placed 120 mm from an obstacle (rectangular absorbing medium, 2). (b) Ray diagram and detector view for biconvex lens placed 57.5 mm from the obstacle. (c) Ray diagram and detector view for biconvex lens placed 3 mm from the obstacle. Note: 1 is a point source illumination, 2 is a rectangular obstacle (10 mm X 0.05 mm, absorbing medium), 3 is a biconvex lens (125 mm focal length, 25 mm diameter) and 4 is the detector. The distance between point source and obstacle is fixed at 5 mm for all the measurements. The detector is placed at the same position during all measurements. Both YZ and XZ views of the optical simulation are given for a, b and c.

Biomedical Optics EXPRESS

As a first step, to address the advantage of using axicon lens over the conventional lenses such as plano convex or biconvex lenses (with long focal length) for performing imaging behind obstacle as proposed in this study, both optical simulation and experiments were performed. Zemax optical simulation of a point source imaged behind an opaque obstacle using a conventional lens is shown in Fig. 2. In order to mimic an obstacle during imaging a rectangular rod (10 mm X 0.05 mm) of 100% absorption is placed in the center of the light path between the object and the imaging end (in the FOV) at various distances. The simulation results show that a conventional lens can only image behind an obstacle when the sample to be imaged is kept at the focus spot or near to the focus depending on the DOF of the lens. It is evident from Fig. 2(b) and 2(c), when the sample is out of focus, the detector view is clearly blocked by the obstacle. In contrast, Zemax simulation given in Fig. 3 illustrates that an axicon lens with an extended DOF can image behind such opaque obstacle for samples placed at different imaging plane. Notably, even when the axicon lens is kept close to the obstacle or imaging object (Fig. 3(c)), the imaging behind obstacle is possible. The optical simulation is further corroborated with experiments. In Visualization 1, comparison of a conventional large DOF lens with an axicon lens using USAF chart as the object is demonstrated. From these results, it is evident that unlike an axicon lens, it is impossible for the conventional lens to image an object at all points from the lens surface to its focal position (while keeping the object still in focus). Both simulation and experimental results clearly demonstrate that axicon has significant advantages over a conventional lens when imaging behind obstacle at different positions.

Biomedical Optics EXPRESS

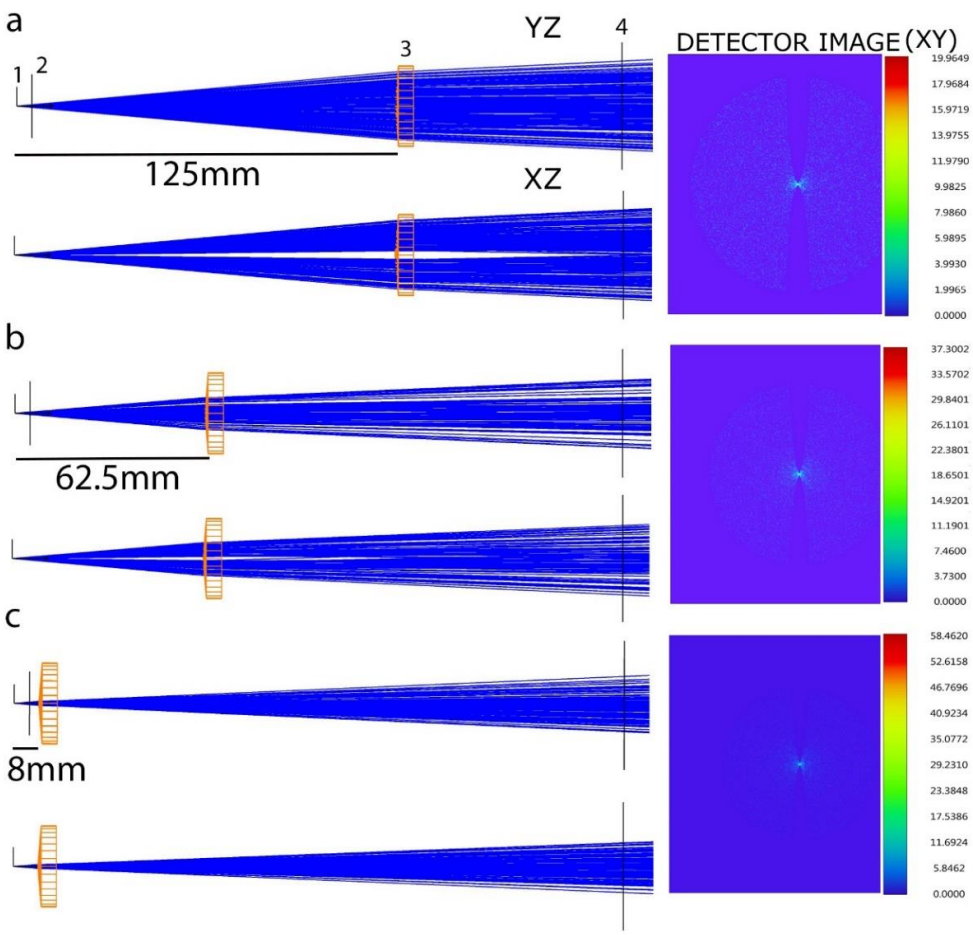

Fig. 3. Illustration of image formation (point source) behind an obstacle for axicon at different focus depth. (a) Ray diagram and detector view for axicon lens placed 120 mm from an obstacle (rectangular absorbing medium, (b) Ray diagram and detector view for axicon lens placed 57.5 mm from the obstacle. (c) Ray diagram and detector view for axicon lens placed 3 mm from the obstacle. Note: 1 is a point source illumination, 2 is a rectangular obstacle (10 mm X 0.05 mm, absorbing medium), 3 is an axicon lens (25 mm diameter) and 4 is the detector. The distance between point source and obstacle is fixed at 5 mm for all the measurements. The detector is also placed at the same position during all measurements. Both YZ and XZ views of the optical simulation are given for a, b and c. The axicon apex angle is oriented towards the point source (left side).

3.2 White light reflection and trans-illumination imaging behind an opaque obstacle

Figure 4 present images of USAF resolution chart behind various opaque obstacles having different shapes, sizes and texture in real time using an axicon lens in the reflection scheme. (The schematic diagram of the reflection setup is shown in Fig. 1(a)). Figure 4(a) and 4(b) shows the USAF resolution chart behind an Allen key of thickness 0.7 mm and behind a surgical needle of thickness 0.35 mm imaged using the proposed method. Image formation of USAF chart elements behind plastic pinhead coated with paint having a thickness of 3.5 mm is illustrated in Fig. 4(c). Figure 4(d), further illustrate USAF chart imaged behind a metallic pin of size 0.5 mm. It is also noted that images of the sample behind obstacles as big as 0.7 mm are achieved even when obstacles are placed as close as 0.5 mm from the USAF chart.

Biomedical Optics EXPRESS

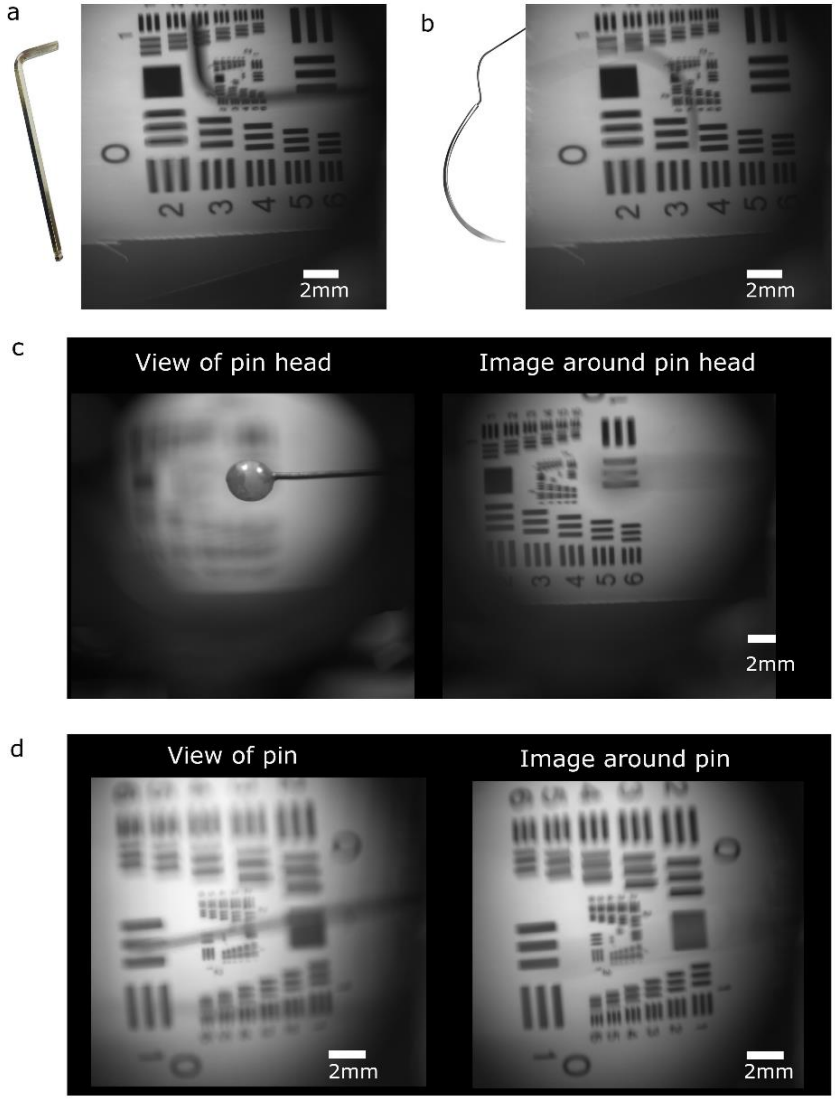

Fig. 4. Imaging behind obstacles using white light reflection method. (a) Image of USAF chart elements behind Allen key of thickness 0.7 mm, placed at a distance of 0.5 mm from the USAF chart. (b) Image of USAF chart elements behind surgical needle (eye) of thickness 0.35 mm, placed at a distance of 0.5 mm from the USAF chart. (c) Image of USAF chart elements behind pin head of 3.5 mm thickness placed at a distance of 3 cm from the USAF chart. (d) Image of USAF chart elements behind pin 0.5 mm thickness placed at a distance of 0.5 mm and 3 cm from the USAF chart.

Biomedical Optics EXPRESS

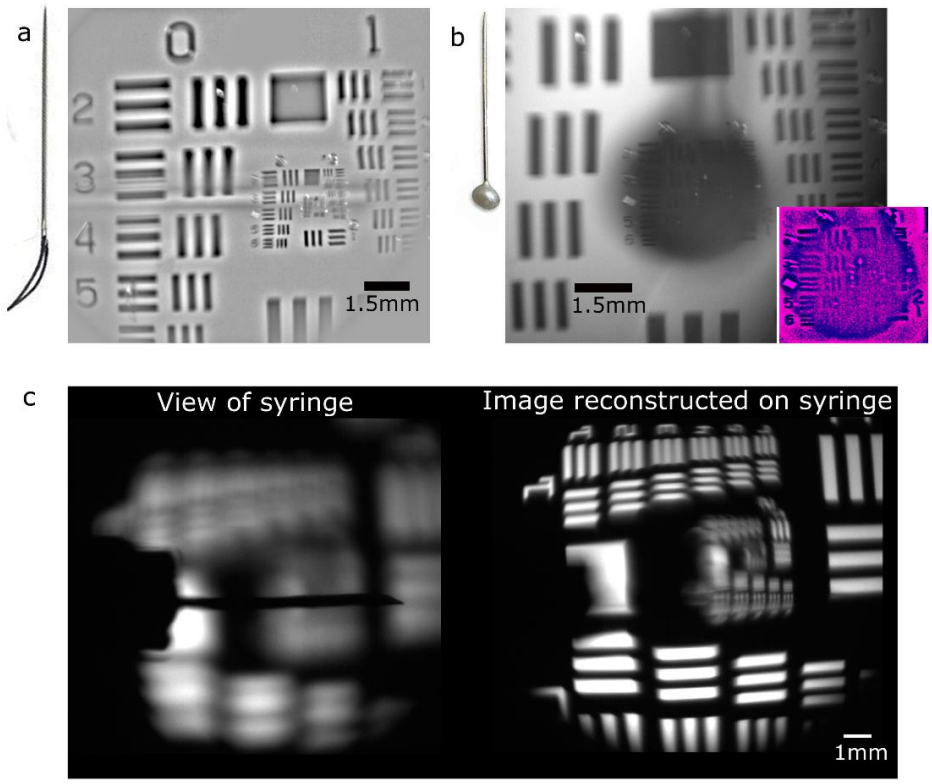

Fig. 5. Imaging behind opaque obstacles using transillumination method. (a) Image of USAF chart elements behind a stitching needle of thickness 0.6 mm. (b) Image of the USAF chart elements behind a paper pin head of thickness 3.5 mm. The inset shows pin head region processed to enhance the contrast to see reconstruction with better clarity. (c) Image of USAF chart elements behind a syringe needle of 0.35 mm thickness.

Similar imaging behind opaque obstacles using axicon is demonstrated in trans-illumination configuration (Fig. 5). (The schematic diagram of the trans-illumination setup is shown in Fig. 1(b)). Figure 5(a) and 5(b) show the obtained imaging results using USAF resolution chart as the test samples kept behind a stitching needle of thickness 0.6 mm and a metal pin head of thickness 3.5 mm, respectively. Further, the processed image is shown as an inset with higher contrast in Fig. 5(b). Image formation of USAF chart elements behind the surgical needle having a thickness of 0.35 mm is illustrated in Fig. 5(c). It is to be mentioned that the axicon position has to be optimized with respect to the sample in order to get the image reconstructed without the obstacle masking it. (By optimization we mean the position of axicon lens with respect to the obstacle). So for different obstacle depending on their size, the position of axicon has to be optimized. These results confirm that axicon lens can be used to image behind obstacles in white light using simple reflection or trans-illumination configuration.

3.3 Fluorescence imaging behind opaque objects

The schematic diagram of the laser based fluorescence imaging system using axicon lens is illustrated in Fig. 1(c). Bessel like beam was generated by propagating a Gaussian beam through an axicon lens. The Bessel beam thus generated is used to illuminate the sample. Both

Biomedical Optics EXPRESS

the illumination and imaging are carried out through the same axicon lens. A high pass filter (above 500 nm) is used in the fluorescence imaging mode to discard the excitation beam and to avoid the shadow effects.

Figure 6(a) shows elements in the 1951 USAF resolution chart behind a paper pin of thickness 0.5 mm imaged in real time (This result is corroborated further with video proof shown in Visualization 2). The feasibility of imaging through the opaque object is further demonstrated by imaging mouse kidney cell clusters behind an Allen key of thickness 0.7 mm (Fig. 6(b)). Inset is the image processed region of the imaged area, in Fig. 6(b) is an image with enhanced contrast. The above illustrations validate the proposed concept and methodology that such small structures can be imaged even when there are opaque obstacles between the sample and imaging unit.

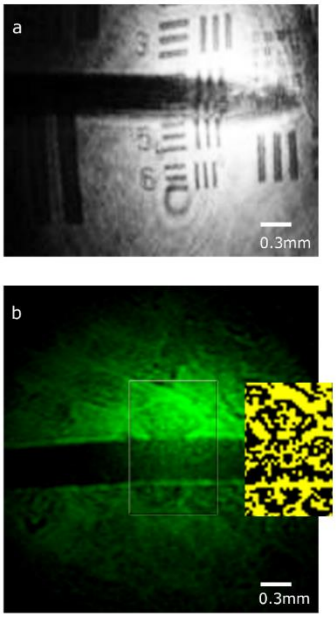

Fig. 6. Illustration of image formation behind obstacles using a laser. (a) Image formation of USAF chart elements behind syringe needle of 0.35 mm thickness. This imaging is performed in reflection mode. (b) Image of cell clusters behind Allen key of thickness 0.7 mm. This imaging is performed in fluorescence configuration. The inset shows the highlighted region (laser spot) in Allen key which is processed to enhance the contrast of the image formed behind Allen key. Basic brightness, contrast and filtering ('unsharp mask') adjustments using ImageJ software were performed as part of the image processing.

Biomedical Optics EXPRESS

3.4 Axicon-objective lens unit

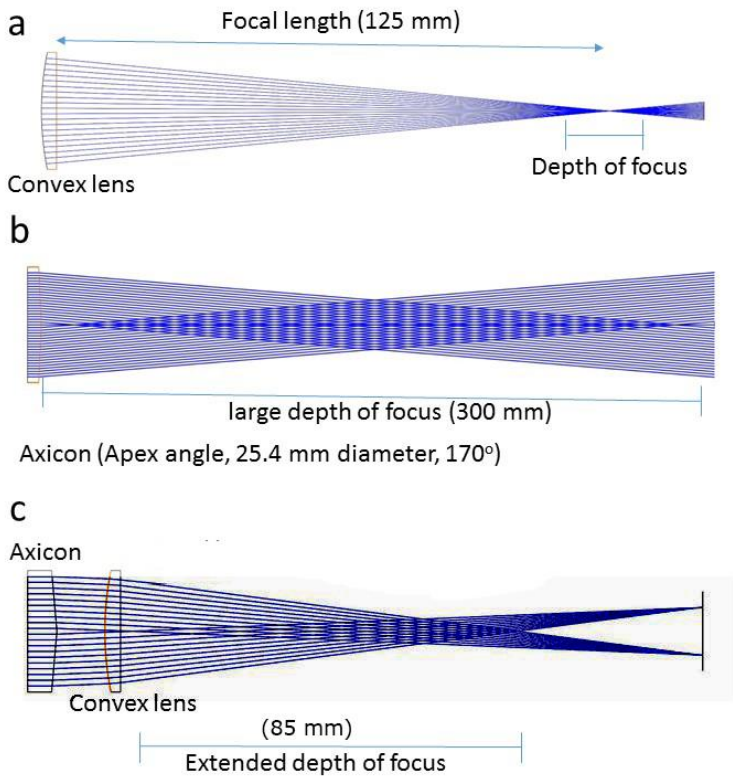

Fig. 7. Illustration of extended focus depth by a combination of the axicon and conventional lens using Zemax simulations. (a) Ray diagram of the conventional plano-convex lens (LA1986 - N-BK7 Plano-Convex Lens, F = 125 mm, Thorlabs) with shallow focus depth (focal length 125 mm). (b) Ray diagram of axicon lens. (c) Ray diagram of combined axicon (170°) and plano-convex lens demonstrating extended DOF. The distance between axicon and convex lens is 10 mm.

The imaging method described in previous sections using an axicon lens has poor image resolution (Fig. 4 and Fig. 5). As described in the above section, a conventional lens (objective) cannot image behind an obstacle at different imaging planes in real time as compared to an axicon. We have introduced an axicon lens close to the conventional lens so as to increase DOF (see Fig. 7). This overall increase in DOF allow the combined axicon-conventional lens unit to image behind obstacle kept at different planes (not possible with same conventional lens alone, Fig. 2). This result is demonstrated with Zemax simulation, Fig. 8. With this concept, we developed the imaging system with combined axicon–microscopic objective (10X, 0.25 NA, Newport) lens unit, which can perform imaging behind an obstacle with higher resolution (Fig. 8(d)).

In order to prove the improved overall resolution of the axicon-objective lens unit, as compared to single axicon lens, we have given images of USAF 1951 resolution test charts in Fig. 9. It is evident from these images that the axicon lens combined with objective lens unit can resolve group 7 element 6 of USAF test chart, which has a line thickness of 2.19 µm.

Biomedical Optics EXPRESS

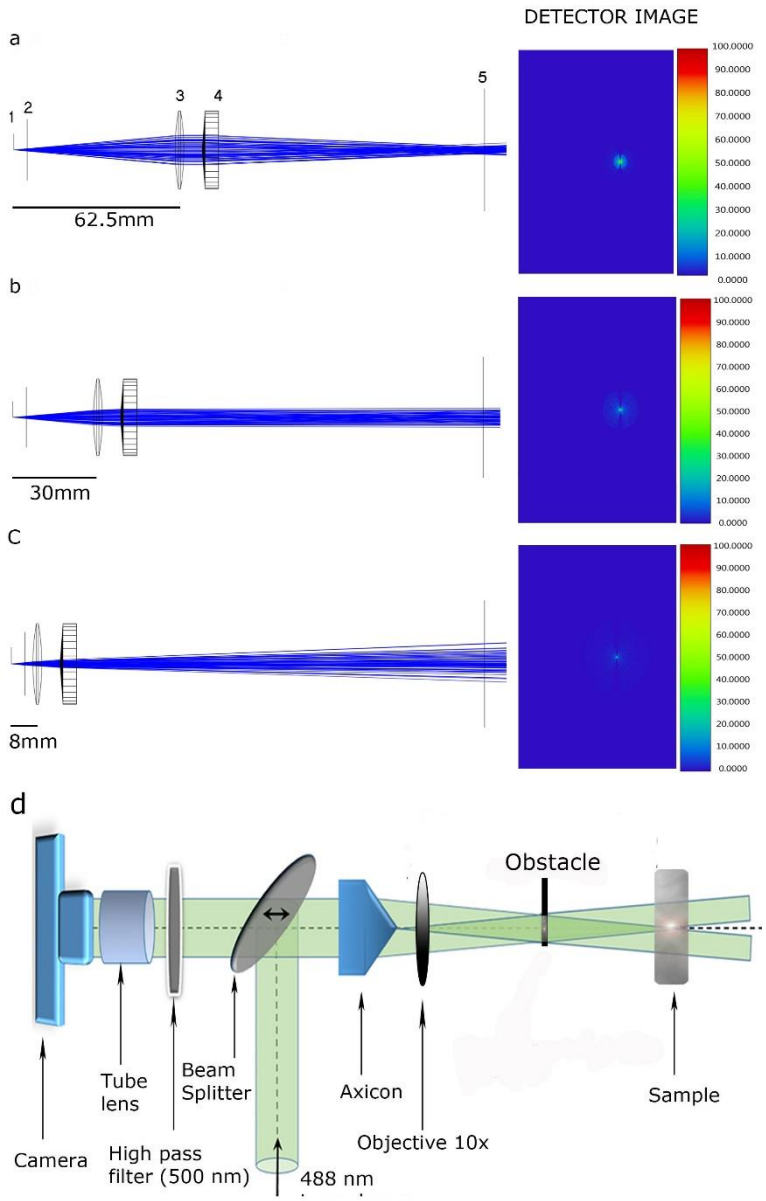

Fig. 8. Zemax simulation and optical setup of the axicon and a conventional lens unit (LB1904 - N-BK7 Bi-Convex Lens, f = 125 mm, Thorlabs). (a) Ray diagram and detector view for lens unit placed 57.5 mm from an obstacle (rectangular absorbing medium, 2). (b) Ray diagram and detector view for lens unit placed 25 mm from the obstacle. (c) Ray diagram and detector view for lens unit placed 3 mm from the obstacle. (d) Schematic diagram of imaging setup using a combination of the axicon and objective lens. Note: 1 is point source illumination, 2 is a rectangular obstacle (10 mm X 0.05 mm, absorbing medium), 3 is a biconvex lens (25 mm diameter), 4 is axicon lens (25 mm diameter) and 5 is the detector. The distance between point source and obstacle is fixed at 5 mm for all the measurements. The distance between axicon and the conventional lens is fixed at 10 mm. The detector is also placed at the same position during all measurements.

Biomedical Optics EXPRESS

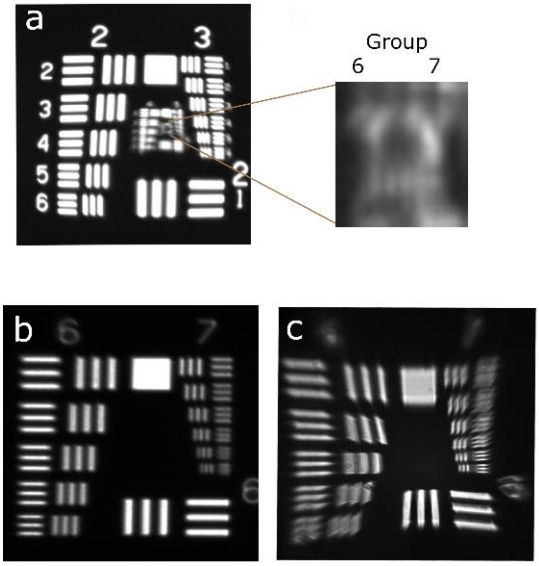

Fig. 9. Comparison of resolution for axicon lens and combined axicon objective lens unit. USAF 1951 test chart imaged through (a) axicon lens (Inset shows group 6 and 7 not resolved). (b) 10x objective lens and (c) combined axicon- 10x objective lens unit (this image shows that group 6 and 7 elements are resolved by combined lens unit).

Further to validate the overall improved resolution of the axicon-objective lens unit, a sequence of mouse kidney cells were imaged behind 60 µm hair in real time, using this microscope configuration Fig. 10 (see also Visualization 3). Additionally, we also provide Visualization 4 demonstrating the reconstruction of kidney cells behind 200 µm thread. Further to validate that the swirling caused due to axicon lens in the combined lens unit does not impact the imaging, we have imaged a region of kidney cells with an objective lens (10x) and compared the same region imaged with a combined axicon- objective lens unit. The result shows no significant effect of swirling contributed by the axicon lens on the kidney cell images (Fig. 11).

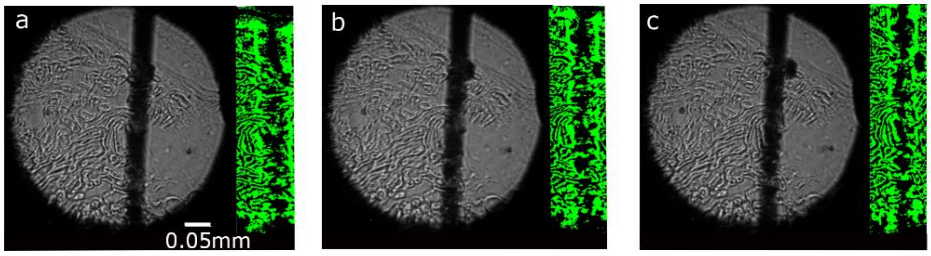

Fig. 10. The sequence of mouse kidney cells (microscopic) raw image formed behind hair. (a-c), illustrate the movement (towards right side) of cells behind a hair of thickness 60 µm. Each image has an inset attached to it showing specifically the imaged region of interest (ROI) with improved contrast.

3.5 Real time imaging behind a needle during surgical insertion

The robustness and versatility of the conceived idea are demonstrated by simulating a surgical injection ambiance. We are first presenting a video to explain the concept of imaging the sample blocked by the surgical needle using white light in real time (Visualization 5). It is evident from the Visualization 5, that irrespective of the movement of the sample (object to be imaged) or needle (obstacle), it is still possible to image the sample clearly behind the needle.

Biomedical Optics EXPRESS

This method allows the precise positioning of the needle on the sample. This is achieved due to the extended DOF of the axicon lens. In this configuration, the shadow can be observed when the sample is very close to the object. However, it doesn't affect the imaging significantly (Visualization 5).

Additionally, this is further validated also in fluorescence configuration. In this experiment, a fluorescently stained biological specimen is kept behind a surgical needle (0.35 mm) and the image of the sample, kept behind the needle, was found to be forming in real time. The raw image sequence of needle insertion is shown in Fig. 12. It is important to note that in the fluorescence imaging method there is no shadow effect present. It can be inferred that though the insertion of the syringe needle was slow, the needle could not be seen due to the image formation of the sample, which is the basic principle of the proposed method. Most importantly, since the needle (obstacle) does not block the FOV, by this technique precise positioning or insertion of the needle is achieved.

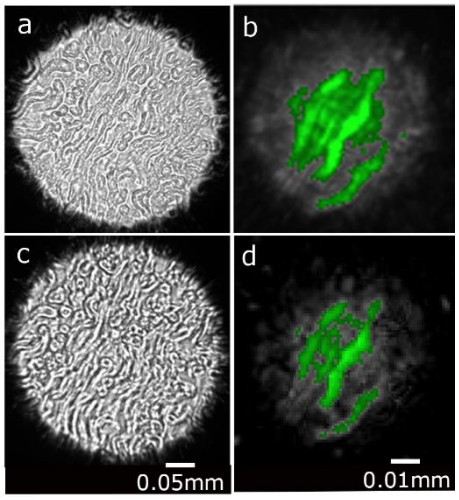

Fig. 11. Comparison of image quality through 10x objective and 10x objective - axicon lens unit. (a) White light image of mouse kidney cells imaged through the 10x objective lens. (b) The region of mouse kidney cell image (fluorescence) using laser through the 10x objective lens. (c) White light image of mouse kidney cells imaged through a combination of 10x objective- axicon lens unit. (d) The region of mouse kidney cell image (fluorescence) using a combination of the 10x objective - axicon lens unit. Note both images (a-c) and (b-d) are taken exactly from the same location of the sample.

4. Discussion

Optical imaging behind opaque obstacles is a long sought after goal with important applications in many fields. Recently, there have been a lot of advancements in imaging techniques to see through scattering or turbid media such as wavefront shaping [6, 22], ghost imaging [23] and adaptive optics technology [24, 25]. These techniques have found potential applications in numerous fields such as astronomical observations, microscopic imaging in turbid tissues and non-destructive testing of defects in microelectronic devices [26, 27]. Viewing through turbid media is challenging due to the fact that the random refractive index variations within the turbid media distort the spherical wavefronts generated by every point source, resulting in a smeared image formation. Though these studies have focused on imaging through turbid or highly scattering media, imaging behind opaque obstacles still remain challenging in biomedical diagnostic imaging, both *in vitro* and *in vivo*.

Biomedical Optics EXPRESS

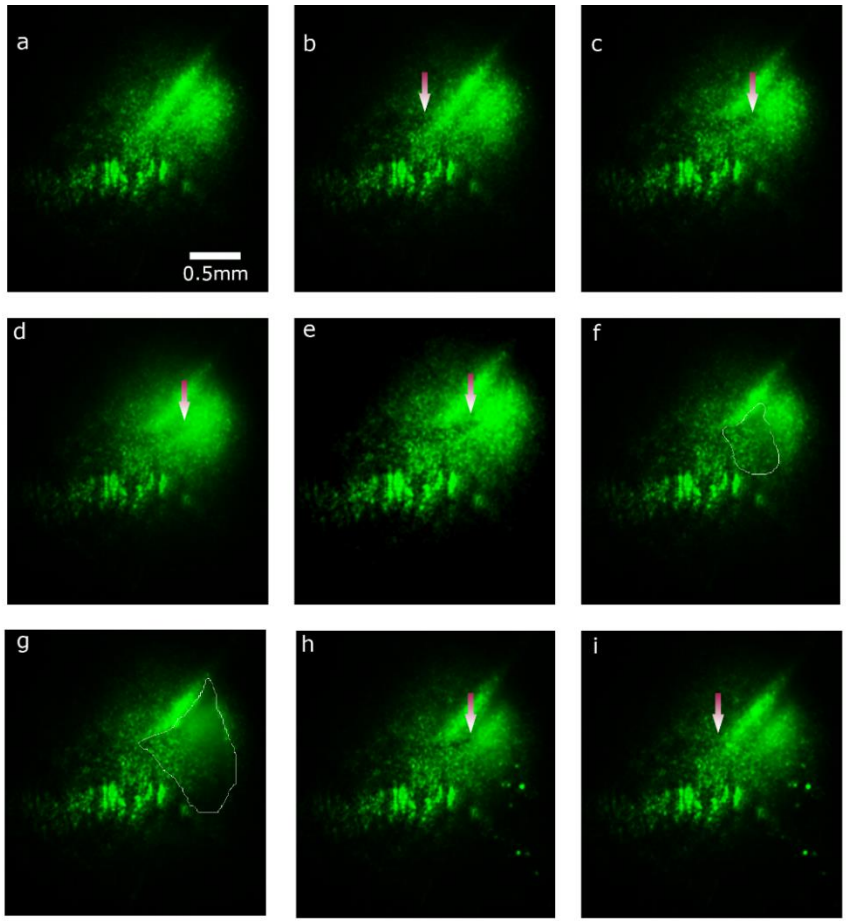

Fig. 12. Illustration of image formation behind surgical needle during insertion. (a-c), Shows the movement of syringe needle kept in front of the biological sample. (d-e), Shows the insertion of the needle into the sample. (f-g), Fluid (stained) is injected into the sample. (h-i), Illustrate the retrace path of the needle after injection. The arrow in images shows the tip of the surgical needle. Note the video also is provided for the same experiment (see Visualization 6).

In this manuscript, we have presented the use of an axicon lens in the proposed configuration to image samples behind obstacles in real time. Using white light and laser light as the illumination sources, the phenomenon of image formation behind obstacle is demonstrated. The method was analyzed in transillumination, reflection and fluorescence configurations. Using this approach, we have performed imaging behind different opaque objects such as Allen key, syringe needle, metallic pin, hair and thread. It is important to note that these objects had different shapes and sizes. It is to be mentioned that the axicon position has to be optimized with respect to the object in order to get the image behind the obstacle. So for different obstacle depending on their size, the position of axicon has to be changed. Axicon lens aperture should be larger than the obstructed object to capture rays behind the object

Using Zemax, we have simulated imaging of a point source obstructed by a rectangular object (10 mm X 0.05 mm, absorbing medium 100%) which was placed within the FOV of the detector. Here, we compared the performance of conventional lens (LA1986 - N-BK7 Plano-Convex Lens, f = 125mm, Thorlabs) and axicon lens (AX255-A, Apex angle 170°, Material: UVFS, Thorlabs) as the imaging arm. The aperture size used for conventional lens and axicon was same. As compared to a conventional lens with fixed focus point, axicons

Biomedical Optics EXPRESS

with apex angle 170° have larger DOF (axicon lens has no focus point unlike conventional lenses). It is important to note that imaging plane can be from the surface of the axicon lens to different planes along very long DOF (Fig. 3). In contrast, it is impossible for a conventional lens to image an object at all points from the lens surface to its focal position (Fig. 2). This simulation result was further verified with experiments (Visualization 1), to emphasize this relevant point.

What are the challenges of using axicon lens as an imaging optical element in microscopy? Obvious reason is due to their low numerical aperture compared to microscopic objectives. It is evident from Fig. 9 that smaller elements in the USAF chart were not resolved through axicon lens. Additionally, slight swirling effect introduces distortion at the central focus region (Fig. 9(c)). Another reason is an axicon easily succumbs to an aberration in the case of oblique or off axis illumination [28].

In this study, to perform imaging behind an obstacle with the improved resolution, we have combined a single axicon with an objective lens to form a combined unit (Fig. 8(d)). The image taken by combined axicon and objective lens unit were similar to the image taken using the single objective lens (see Fig. 11). It is important to note after combining the lenses, the imaging plane starts to form from the surface of the conventional lens (Fig. 7.). This result was further corroborated by performing Zemax optical simulation for imaging behind an obstacle with the combined lens unit. The result is shown in Fig. 8. It is evident from the results that, the combined unit allowed the point source to be imaged at the detector even when the obstacle was placed at multiple positions (beyond the DOF of the conventional lens). This imaging feature was not possible when only a single conventional lens was used (Fig. 2). By this approach, we have demonstrated that imaging resolution is improved with combined lens unit as compared to the earlier imaging system using single axicon lens (Fig. 9 and Visualization 3).

In a notable research work, paraxial ray optics cloaking is demonstrated in the visible regime using lens array by John C. Howell *et al.* [29]. However, one of the main limitation is the sample to be cloaked should be placed between the cloaking devices (optical device assembly) and not near the background or sample to be imaged. Moreover, this method has not been adapted into any microscopic configuration. On the contrary, we have demonstrated imaging behind an obstacle in microscopic configuration. Comparing with paraxial cloaking method, our imaging technique is also different, as imaging magnification is not one.

In our study, we are not manipulating (bending or stretching) the optical rays neither changing the environment of the obstacle or using additional optical components to change the ray path as in conventional optical cloaking methods [30–35]. Instead, using a larger DOF of the axicon, we have demonstrated that it is possible to image the sample behind an obstacle at different DOF, irrespective of the position of obstacle or sample position. From this perspective, we have also demonstrated the imaging of biological sample behind surgical syringe needle as a proof of concept (Visualization 5 and Visualization 6).

An earlier study by Bouchal *et al.* showed that an ideal nondiffracting beam can exactly reconstruct its initial intensity profile behind an obstacle of arbitrary form and size [20]. Importantly in this study, illumination is done through an axicon lens and collection is done separately via a camera which introduced shadow effects. However, it is important to note that, in our approach, we are performing illumination and imaging through the same axicon lens (Fig. 1). This means either the reflected or fluorescence light from the object is imaged by the camera through the axicon lens behind the obstacle. The reflected or fluorescence light from the object will not have self-healing properties. (Only the excitation beam through axicon can become a nondiffracting beam). Additionally, we have demonstrated this imaging concept using white light transillumination setup. All these experiments and observed results clearly show that the focusing plane of the axicon lens is the key contributor and not the non diffraction beam property of illumination to image behind the obstacle. For reflection

Biomedical Optics EXPRESS

configuration shadow of the objects can be observed. However, the shadow can be eliminated in fluorescence scheme with the help of emission filter.

Diagnostic medical imaging significance: The field of view of imaging systems used during microsurgery is restricted to the field of view of the microscope/imaging modality. As mentioned earlier there are instances where the surgical tools obstruct the field of view, especially when dealing with extremely small structures. It is possible to cause damage from surgical instruments unless the surgeon is always aware of the position of the targeted structures in the surgical site. From this perspective, we have here demonstrated the proof of concept of seeing the structures below the needle during surgical injection (Visualization 5 and Visualization 6). Using this technique, it is illustrated that the needle can be inserted at the precise location, thereby reducing the number of needle injuries.

5. Summary

In this manuscript, we have demonstrated a method for imaging behind the opaque obstacle and its potential application in guided *in vitro* needle placement. It is envisaged that this simple and cost effective optical configuration described here can introduce a paradigm shift in the way imaging behind opaque obstacles is performed. Further, such an approach can offer a wide range of potential applications in a variety of fields such as diagnostic imaging, theranostics, microsurgery, to name a few.

Funding

The authors acknowledge the financial support received from Ministry of Education (MOE-AcRF RG162/15) and MOE-AcRF RG98/14. One of the authors, A.S. thank the financial support by NTU as research student scholarship award.